Transactions of the Korean Nuclear Society Autumn Meeting
Pyeongchang, Korea, October 30-31, 2014

Experimental investigation on the droplet entrainment from interfacial waves in air-water horizontal stratified flow

Byeong-Geon Bae[1], Byong-Jo Yun[1*], and Kyoung-Du Kim[2]
[1]*Mechanical Engineering Department, Pusan national Univ., Jangjeon-dong, Guemjeong-gu, Busan, 609-390, Korea*
[2] *Korea Atomic Energy Research Institute, 1045 Daedeok-daero, Yuseong-gu, Daejeon, 305-353, Korea*
**Corresponding author: bjyun@pusan.ac.kr*

1. Introduction

The SPACE code is being developed for the safety analysis code of the Korean nuclear power plants. Unlike the conventional safety analysis codes using two-fluid model, the SPACE code adopts three governing equations for gas, continuous liquid, and dispersed droplet fields. The amount of droplet entrainment is very important because of significant effects on the heat and mass transfer between liquid and gas phases in the Nuclear Power Plant (NPP).

Up to now, many constitutive relations for the gas and continuous liquid fields have been developed by previous investigators. On the contrary, available constitutive relations for the droplet fields are very limited. Moreover, most existing models for the droplet entrainment are developed for the application in the vertical annular flow. It was mainly due to the fact that droplet entrainment affects the Peak Cladding Temperature (PCT) of the nuclear fuel rod in the Postulated accident conditions of NPP. Recently, droplet entrainment in the horizontally arranged primary piping system for the NPP is of interest because it affects directly the steam binding phenomena in the steam generators. Pan and Hanratty correlation is the only applicable one for the droplet entrainment rate model for horizontal flow [1]. Moreover, there are no efforts for the model development on the basis of the droplet entrainment principal and physics phenomena. More recently, Korea Atomic Energy Research Institute (KAERI) proposed a new mechanistic droplet generation model applicable in the horizontal pipe for the SPACE code [2]. However, constitutive relations in this new model require three model coefficients which have not yet been decided.

The purpose of present work is determining three model coefficients by visualization experiment. For these model coefficients, the major physical parameters regarding the interfacial disturbance wave should be measured in this experiments. There are the wave slope, liquid fraction, wave hypotenuse length, wave velocity, wave frequency, and wavelength in the major physical parameters. The experiment was conducted at an air-water horizontal rectangular channel with the PIV system. In this study, the experimental conditions were stratified-way flow during the droplet generation. Three coefficients were determined based on several data related to the interfacial wave. Additionally, we manufactured the parallel wire conductance probe to measure the fluctuating water level over time, and compared the wave height measured by the parallel wire conductance probe and image processing from images taken by high speed camera.

2. Droplet entrainment model proposed by KAERI

The droplet generation phenomena from the continuous liquid into the gas field appears by various mechanism. Depending on the flow velocity of gas and liquid, the hydrodynamic force leads to the deformation of phase interface wave in two-phase flow. Under the certain conditions, droplets with the large waves can be generated. Ishii & Grolmes classified five droplet generation mechanisms [3]. These five mechanisms are shown in Fig. 1. A new droplet generation model developed by KAERI is based on the first type among five mechanisms.

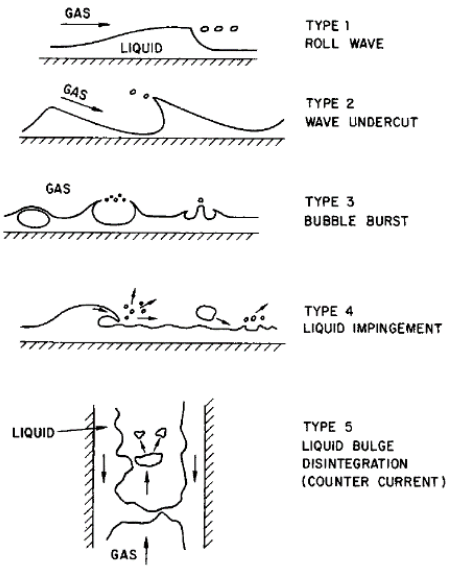

Fig. 1 droplet entrainment mechanism
(Ishii & Grolmes, 1975)

The first mechanism is that the shear force causes mainly the droplet generation on the interfacial large roll wave. The droplet entrainment rate per unit length of channel is given as:

$$M'_{DWSC} = \frac{\Delta Z}{\lambda_{DW}} \times m_{SC} \times \frac{f_{DW}}{\Delta Z} \qquad (1)$$

The m_{sc} is the mass of the droplet entrainment by shear force, λ_{DW} is the wavelength, f_{DW} is the wave frequency and ΔZ is unit length of channel. The mass of the droplet entrainment in Eq. (1) is composed of the shear

force, surface tension and the gravity, which satisfy the momentum balance equation expressed by:

$$m_{sc}g + \bar{\sigma}_i L\cos\theta = \bar{\tau}_i A_i \sin\theta \qquad (2)$$

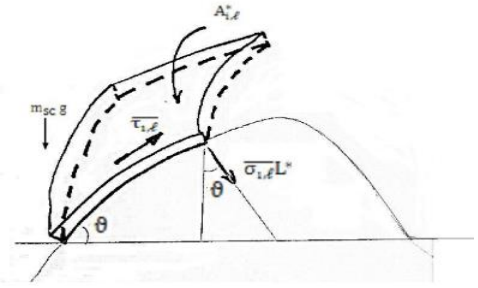

Fig. 2 The interfacial wave by shear force

Where, θ is the interfacial wave angle for droplet entrainment, g is the gravity constant, $\bar{\sigma}_i$ is the surface tension, $\bar{\tau}_i$ is the interfacial shear stress, L is the surface perimeter of the interfacial wave for surface tension, and the A_i is the surface area of the interfacial wave. Among these parameters, the surface area and the surface perimeter on the wave are related to K_1, K_2 of three model coefficients. Eq. (3) and (4) are the applicable equations for two coefficients when the droplet is generated.

$$A_i = K_1 \lambda_{DW} \alpha_l D_H \qquad (3)$$

$$L = \sqrt{A_i} \times \left(\frac{1}{R_1^*} + \frac{1}{R_2^*}\right) = \sqrt{K_1 \lambda_{DW} \alpha_l D_H} \times \left(\frac{D_H}{\lambda_{DW}} + \frac{1}{\infty}\right)$$

$$= K_2 \sqrt{\frac{\alpha_l (D_H)^{3/2}}{\lambda_{DW}}} \qquad (4)$$

Eq. (3) is formulated by assuming that the surface area of the interfacial wave is proportional to the multiplication between wavelength and the amount of the liquid. Eq. (4) assumes that the perimeter of the interfacial wave is proportional to the square root of the surface area of the interfacial wave. The R_1^*, R_2^* of the radius of curvature, are the dimensionless parameter. R_1^* is proportional to the wavelength toward flow direction. R_2^* is assumed as the infinity, because the wave shape along lateral direction of the channel is nearly flat. The third coefficient, K_3 is accounting for the droplet entrainment angle, θ. Three coefficients mentioned above can be determined experimentally in the horizontal rectangular channel under air-water stratified flow conditions.

3. Experimental facility

3.1 Test Loop

The test loop consists of a test section, air and water supply systems as shown in Fig. 3. The horizontal rectangular test section of which size is 40 mm × 50 mm × 4.2 m in width, height, and length, respectively, was made with transparent acrylic. This test section is designed for easy observation of the wave configuration. Air and water are supplied to the inlet plenum of the test section by the air blower and the centrifugal pump, respectively. At the outlet plenum of the test section, air and water are separated. And then air is discharged to atmosphere and water recirculates the loop.

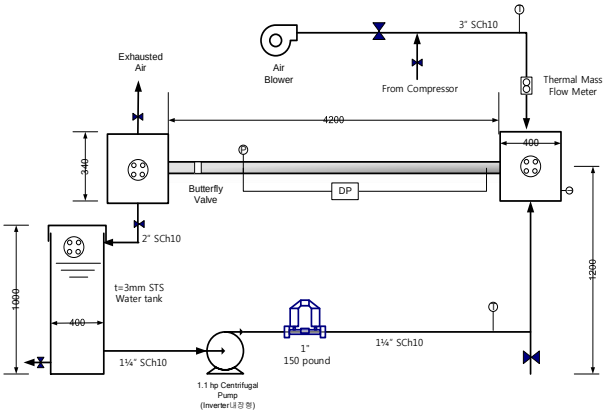

Fig. 3 Schematic diagram of the air-water test loop

The instrumentations for the experiment include the thermal mass flowmeter for the air flow rate, the Coriolis flowmeter for the water flow rate, the thermocouple for the air and water temperature in the inlet pipe, and pressure and differential transducers for the pressure distribution along the test section. In addition to these, PIV equipment and parallel wire conductance probe were applied for the characterization of phase interface waves. Details of these two instruments are explained in the following sections.

3.2 PIV system

The Fig. 4 shows the schematic diagram of PIV(Particle Image Velocimetry) system applied in the present experiments for the visualization and determination of wave characteristics. The Nd:YLF laser beam of which wavelength and power are 527 nm and 20 mJ, respectively, is generated from the laser oscillator. After it passes through the mirror arm and cylindrical lens, it is converted to the plane laser sheet of which thickness is 1 mm.

The spherical seeding particles which are illuminating by laser sheet are added into the water to trace flow. The wavelength of the emitted light from the particles is 570 nm. The high speed camera (Dantec M310) with 1280×800 resolution and 2000 Hz frame rate was used to acquire the images at 3.5 m downstream from the inlet of test section in the experiments. The images were taken from side of test section. The timer box was basically used to trigger both the laser and camera simultaneously. It also applied to trigger the acquisition of signal for parallel wire conductance probe.

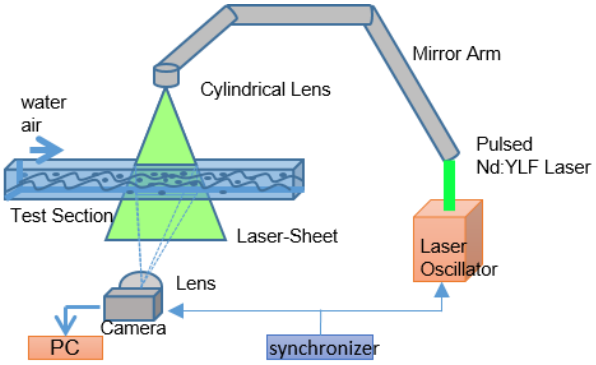

Fig. 4 Schematic diagram of the PIV laser system

3.3 Parallel wire conductance probe

Several techniques have been proposed by previous investigators for the measurement of liquid film thickness. The examples are conductance probe, capacitance probe, optical probe, and needle probe (Clark, [4]). If the water's conductivity was much larger than the air's conductivity, it would be suitable to use the conductance probe. Conductance probe method has the linear relationship between the water level and the resistance of the fluid. There are two types of available conductance probes. One is the parallel wire conductance probe, the other is the flush mounted probe. Their applications are dependent on the thickness of water film. That is, the parallel wire conductance probe is used to measure relatively thick films while the flush mounted probe is capable of measuring very thin film of which thickness is in the order of microns (Sawant et al., [5]). Additionally, when measuring local film thickness, the parallel wire conductance probe is appropriate instead of the flush mounted probe in the present study. Thus, we developed the parallel wire conductance probe for the measurement of the instantaneous wave height in the stratified flow. Fig. 5 shows the photograph of the parallel wire conductance probe developed in the present work. The diameter of each wire consisting of parallel wire is 0.07 mm and gap between two wires are 3 mm. The parallel wire was installed in the center of the test section. Teflon and screw were used to prevent a leakage of water from the flow channel, and spring was used to maintain the constant tension of wires in the flowing condition. The electronic circuit were improved from the design presented by Kang and Kim [6]. By applying the full wave rectifier and smoothing circuit, the applied AC signal was converted into the DC signal. A function generator supplied a 100 kHz carrier signal with 1V. The output voltage range is changed by ratio of two resistance constituted on the OP amp.

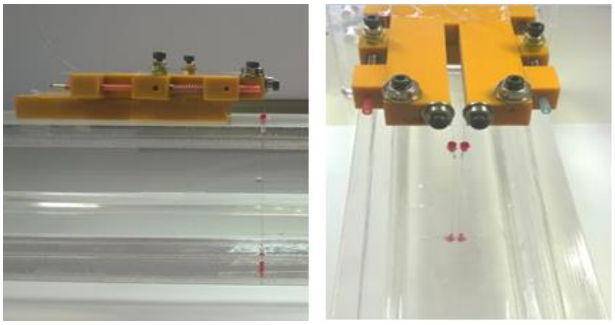

Fig. 5 Photograph of the parallel wire conductance probe

4. Experiments and discussions

4.1 Validation of wave height measurement

For the confirmation of soundness of measured local wave height, we compared the wave height obtained from image method with that of the parallel wire conductance probe. In the test, Sobel algorithm provided by MATLAB was applied for identification of interfacial boundary between two phases. For the development of the parallel wire conductance probe, we have confirmed the linear relationship between water level and fluid's resistance change by COMSOL analysis, in advance. And then, calibration experiments were conducted to confirm the linearity of the output voltage of electronic circuit according to the water level in an air-water stagnant flow condition. As shown in Fig. 6, the maximum linearity is found to be 10%. The output voltage range can be adjustable by changing the resistance for the amplification of the raw signal in the electronic circuit. In case of tap water as working fluid, an order of kΩ is appropriate for the resistance of an amplification circuit, while it is suitable to use the resistance of order of MΩ for demi-water. It is due to that the conductivity of demi-water is much lower than that of the tap water. In this experiments, the 4.7 MΩ resistance was used for the demi-water. The experiments were performed from stratified smooth to wavy flow covering 7 ~ 15 m/s of air superficial velocity and 0.07 ~ 0.1 m/s of water superficial velocity. Fig. 7 shows the comparison of measured wave heights obtained from two methods. A red symbol represents the wave height by parallel wire conductance probe method, and a black symbol is for the wave height by PIV image processing method. As in the Fig. 7(a)-(c), the wave height is increased according to the decrease of the gas superficial velocity. And it also affected by the liquid superficial velocity in Fig. 7(a), (d) and Fig. 7(b), (e). The more liquid superficial velocity is increased, the more wave height is increased.

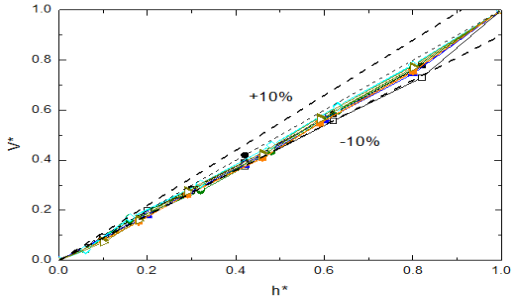

Fig. 6 Dimensionless water level vs. Output voltage in the static experiments

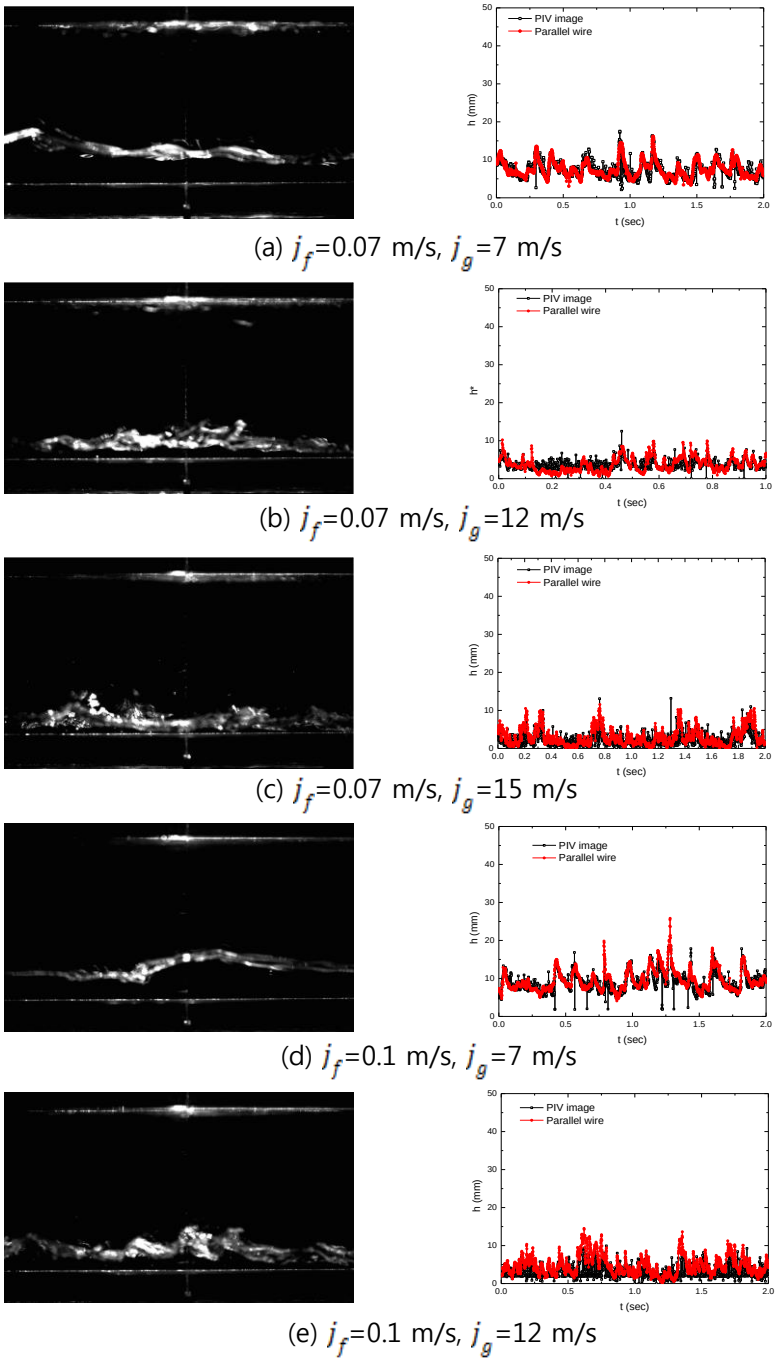

Fig. 7 Comparison of measured water level from parallel wire conductance probe and PIV image techniques

Finally, the comparison of water level confirms that the both measurement techniques are credible for the instantaneous measurement of water level in the present flow conditions.

4.2 Experiments on the wave characteristics

The visualization experiment was conducted when the droplets were generated from the phase interface waves in the stratified flow condition. The inception criterion for the droplet entrainment correlation by Ishii & Grolmes (1975) was applied for the determination of flow conditions. The correlation was based on the droplet generation phenomena in which shear stress plays a major roll against the viscosity force and surface tension on the wave. The flow conditions calculated by this correlation are shown in Manhane et al. (1973)'s flow regime map (see Fig. 8) [7]. Present experiments were carried out at seven flow conditions with different gas and liquid superficial velocities predicted by Ishii & Grolmes correlation. The experimental conditions are plotted with the triangular symbols in Fig. 8 and also tabulated in Table 1. The experimental data were taken at the 3.5 m from the inlet of the test section. In the tests,

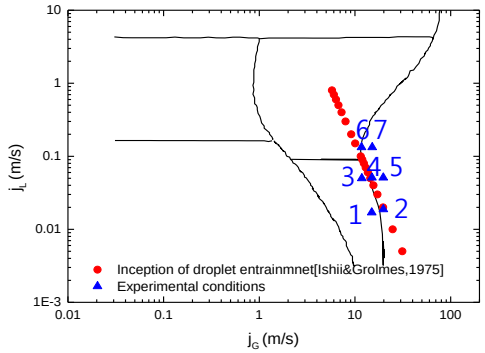

Fig. 8 Flow regime map of experiments

the fluids temperatures and pressure were maintained constantly at room temperature and atmospheric pressure, respectively, and pressure difference along the test section was negligible.

Table 1. Summary of experimental conditions

	j_g (m/s)	j_f (m/s)
Case1	14.98	0.018
Case2	19.8	0.019
Case3	11.8	0.05
Case4	15.04	0.051
Case5	19.75	0.051
Case6	11.7	0.133
Case7	15.15	0.133

The Fig. 9(a)-(f) show the measured results of the parameters related to characteristics of interfacial waves from experiments. The parameters are required for the determination of three coefficients for the newly proposed droplet entrainment model. As shown in Fig. 9(a)-(f), the x-axis of each graph means the gas Reynolds number. Here, the Re_f and Re_g mean Reynolds numbers for liquid film and gas flow, respectively, defined by each phasic superficial velocity. The y-axis, are for the (a) wave slope, (b) liquid fraction, (c) wave hypotenuse length, (d) wave frequency, (e) wave velocity, and (f) wavelength, respectively. The wave slope is increased with the increase of Reynolds number for liquid film and is in the range of 20~30 degree as in Fig. 9(a). The liquid fraction during the droplet generation from the interfacial wave has higher value with the higher Reynolds number for liquid film and lower Reynolds number for gas as shown in Fig. 9(b). The tendency of liquid fraction on the Reynolds number for liquid film is reasonable, because liquid superficial velocity is directly related to the liquid volume flow rate. The Reynolds number for gas has also effect on the change of the liquid fraction because it makes droplet generation arisen by interfacial shear stress. The measured hypotenuse length of the liquid wave shows similar tendency with liquid fraction as in Fig 9(c). From this fact, we can conclude that the liquid fraction increases the large and long wave is formed.

It is reported by previous investigators (Paras et al. (1994), Sawant (2008), Schubring and Shedd (2008)) that the wave frequency is generally increased with the increase of Reynolds number for gas [8], [9]. However,

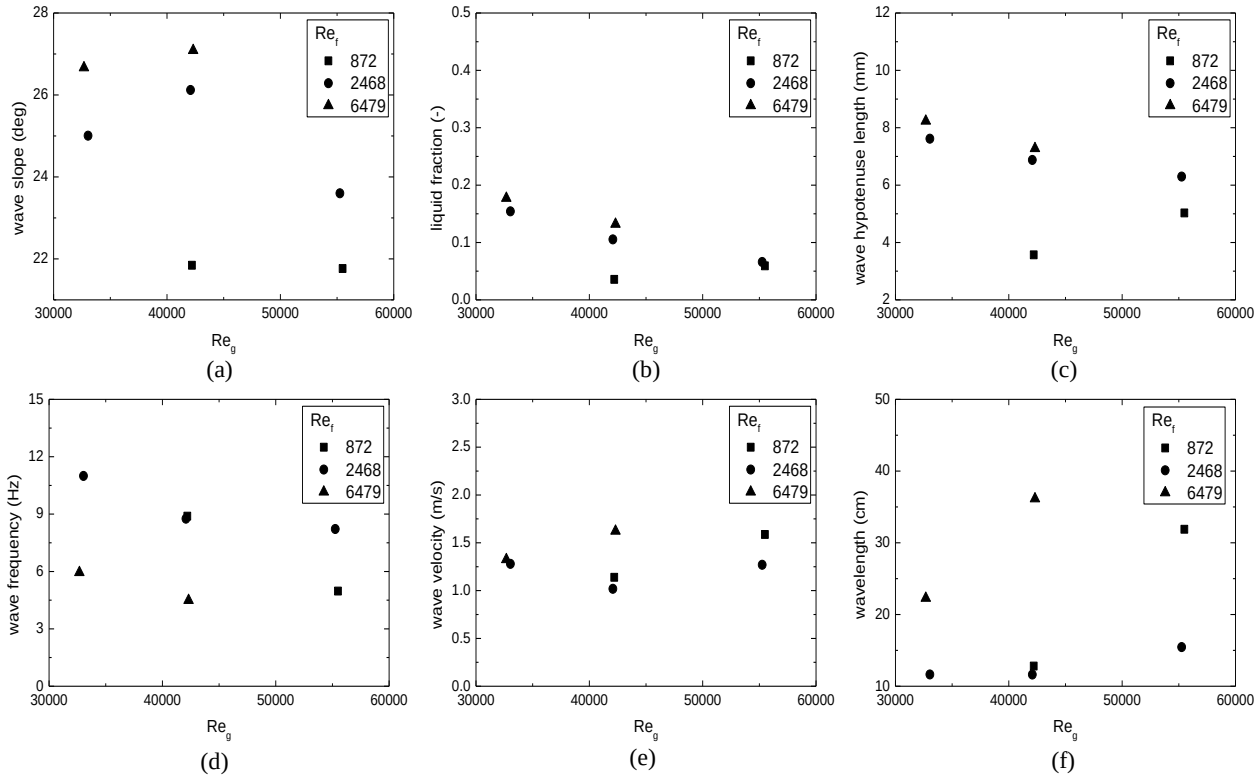

Fig. 9 Experimental results of major parameters regarding the interfacial wave

in the present experimental conditions, the wave frequency is decreased with increase of Reynolds number for gas. It tells us that there exists the transition region from regular waves to irregular waves. The liquid wave velocity is observed in the range of 1~2 m/s as shown in Fig. 7(e). Lastly, the wavelength which is determined by the wave frequency and the wave velocity is increased with the Reynolds number for gas. From these six parameters representing the wave characteristics, we can calculate three model coefficients at given experimental conditions in chapter 4.3.

4.3 Determination of three model coefficients

By using six measured parameters, we determined three model coefficients for the new droplet entrainment model proposed by KAERI. Two model coefficients are presented in Eq. (3), (4) and the other coefficient is the wave slope explained in the previous section. As shown in Fig. 10(a), the measured model coefficient K1 is distributed around 0.4 at given experimental conditions. The model coefficient K2 is increased with the increase of gas Reynolds number in Fig. 10(b). The model coefficient K3 is found to be between 20 and 30 degree in the present experiments as shown in Fig. 9(a). As stated previously, the wave slope is increased with the increase of Reynolds number for liquid film under the certain Reynolds number for gas. And we can presume that the wave slope will be smaller as the flow regime changes from stratified to annular flow conditions. It should be noted here that we determined three model coefficients by assuming two dimensional wave behavior.

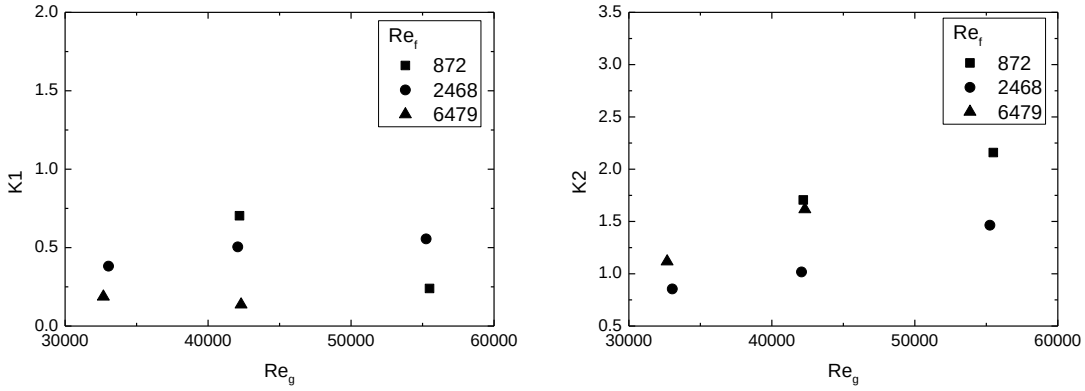

(a) (b)

Fig. 10 the model coefficients K_1, K_2 on seven flow conditions

5. CONCLUSIONS

Experimental investigation was performed for droplet entrainment from phase interface wave in an air-water stratified flow. In the experiments, we measured major physical parameters related to the characteristics of interfacial wave in the horizontal rectangular channel by PIV equipment. There are wave slope, liquid fraction, hypotenuse length, wave frequency, wave velocity, and wavelength in six major parameters.

In case of high gas superficial velocity, unclear interfacial boundary images were observed due to the scattered light on the surface of three dimensional waves. To confirm the exact interfacial boundary, we developed the parallel wire conductance probe. And then we confirmed the water level obtained from PIV images and parallel wire conductance probe. As shown in Fig. 10(a)-(e), the comparison of measured water level from two methods represents good agreement.

By using measured six parameters shown in Fig. 7(a)-(e), we determined three model coefficients required for a newly proposed droplet entrainment model explained in chapter 2. The model coefficients, K_1 and K_2 according to the gas Reynolds number show as in Fig. 8(a) and (b). The K_3 is represented in Fig. 7(a).

Three model coefficients were just results in a restricted experimental conditions. In the following work, the experiment will be performed for extended air-water flow conditions so that we will apply three model coefficients to the SPACE code.

ACKNOWLEDGEMENTS

This work was supported by Nuclear Research & Development Program of the NRF (National Research Foundation of Korea) grant funded by the MSIP(Ministry of Science, ICT and Future Planning) and by the Nuclear Safety Research Center Program of the KORSAFe grant funded by Nuclear Safety and Security Commission (NSSC) of the Korean government (Grant code: NRF-2012M2A8A4055548, 1305011).

REFERENCES

[1] Pan and Hanratty, Correlation of entrainment for annular flow in horizontal pipes, International journal of multiphase flow 28.3, 385-408, 2002.

[2] Park, J. W, The development of droplet entrainment and de-entrainment mechanistic model in horizontal pipe, KAERI report, 2012.

[3] M. Ishii and M. A. Grolmes, Inception criteria for droplet entrainment in two-phase Concurrent Film Flow, AlChE Journal 21, 1975.

[4] Clark,W.W, Liquid film thickness measurement. Multiphase Science and Technology 14, 1–74, 2002.

[5] Sawant, P. *et al*, Properties of disturbance waves in vertical annular two-phase flow, *Nuclear Engineering Design 238*, 3528-3541, 2008.

[6] Kang, H. C. and Kim, M. H, The development of a flush-wire probe and calibration method for measuring liquid film thickness, International journal of multiphase flow 18.3, 423-437, 1992.

[7] J. M, Mandhane. *et al.*, A flow pattern map for gas-liquid flow in horizontal pipes, Int. J. Multiphase Flow. 1, 537-553, 1973.

[8] Schubring, D., and T. A. Shedd. Wave behavior in horizontal annular air–water flow." International Journal of Multiphase Flow 34.7, 636-646, 2008.

[9] Paras, S. V., N. A. Vlachos, and A. J. Karabelas, Liquid layer characteristics in stratified—Atomization flow. International journal of multiphase flow 20.5, 939-956, 1994.